Journal of Power Sources 195 (2010) 532–535

Contents lists available at ScienceDirect

Journal of Power Sources

journal homepage: www.elsevier.com/locate/jpowsour

Short communication

Out-of-cell measurements of H_2–H_2O effective binary diffusivity in the porous anode of solid oxide fuel cells (SOFCs)

Weidong He, Kyung Joong Yoon, Ryan S. Eriksen, Srikanth Gopalan*, Soumendra N. Basu, Uday B. Pal

Department of Mechanical Engineering, Division of Materials Science and Engineering, Boston University, Boston, MA 02215, USA

ARTICLE INFO

Article history:
Received 6 May 2009
Received in revised form 29 July 2009
Accepted 30 July 2009
Available online 7 August 2009

Keywords:
Solid oxide fuel cell
Anode
Effective binary diffusivity
Limiting current
Transport

ABSTRACT

The effective binary diffusivity of H_2 and H_2O in a Ni and yittria-stabilized zirconia (YSZ) anode of the solid oxide fuel cells (SOFCs) was measured between 650 and 800 °C using an electrochemical cell consisting of an oxygen pump, an oxygen sensor, and a porous SOFC anode pellet. The effective binary diffusivity was obtained from the relationship between the current density across the oxygen pump, and the H_2 partial pressure gradient across the anode sample measured using the oxygen sensor. The anode limiting current density and concentration polarization were estimated using the experimental results.

1. Introduction

Solid oxide fuel cells (SOFCs) have gained significant interest due to their high energy conversion efficiency, low pollution emission, modularity, and fuel flexibility. Among the basic designs of SOFCs, the anode-supported SOFCs have been extensively investigated because they exhibit higher cell performance compared to either the electrolyte-supported or cathode-supported designs [1,2]. In the anode-supported SOFCs, the anode concentration polarization is one of the significant contributions to the performance loss, because the thick anode impedes the rapid transport of the gaseous reactant and product species [3,4]. In a thick and porous anode, the gas transport is mainly through a diffusion process [5], and the effective diffusivity of gas species is determined by the anode parameters such as the pore size, volume fraction of pores, and tortuosity. Therefore, it is important to measure the effective diffusivity of gases under the operating conditions of SOFCs in order to effectively engineer the anode microstructure and lower the concentration polarization. Between 30 and 300 °C, the effective diffusivity of mixed gases has been measured using techniques such as gas chromatography [6,7], thermogravimetry [8], and zero length column method [9]. Although the effective diffusivity of O_2 and N_2 in the SOFC cathode has been measured using an electrochemical cell between 650 and 800 °C [10], experimental measurements of the effective binary diffusivity of H_2 and H_2O in the SOFC anode have not been reported to the authors' knowledge. In the present work, the effective binary diffusivity of H_2 and H_2O in a porous Ni and yittria-stabilized zirconia (YSZ) cermet anode was measured using an electrochemical cell comprised of an oxygen pump, an oxygen sensor, and a porous anode sample. The diffusivity values between 650 and 800 °C were obtained from the relationship between the current density across the oxygen pump and the H_2 partial pressure gradient across the porous sample measured using the oxygen sensor. The temperature dependence of the effective diffusivity has been discussed, and the anode limiting current density and concentration polarization have been estimated using the experimental results.

2. Experimental

Fig. 1a shows the schematic of the electrochemical cell to measure the effective binary diffusivity of H_2–H_2O through a porous Ni–YSZ anode. It consists of a dense 6 mol% YSZ tube 3.9 in. long, 0.7 in. in diameter, with a wall thickness of 0.1 in. obtained from McDaniel Advanced Ceramic Technologies, with a dense YSZ disc on one end and a porous Ni–YSZ disc on the other end. A dense YSZ disc was prepared by uniaxial die-pressing of 8 mol% YSZ powder (Tosoh Corp.) followed by sintering at 1400 °C for 8 h. A paste of NiO–YSZ was prepared by mixing NiO (J.T. Baker) and 8 mol% YSZ powder with alpha-terpineol and binder in a desired ratio, and painted on both sides of the YSZ disc and tube to form the electrodes for the oxygen pump and sensor, respectively. A porous Ni–YSZ disc (50 vol% Ni + 50 vol% YSZ) was fabricated by the high shear compaction process [11,12] as described in our earlier work using NiO

* Corresponding author. Tel.: +1 6173582297; fax: +1 6173535548.
E-mail address: sgopalan@bu.edu (S. Gopalan).

0378-7753/$ – see front matter © 2009 Elsevier B.V. All rights reserved.
doi:10.1016/j.jpowsour.2009.07.051

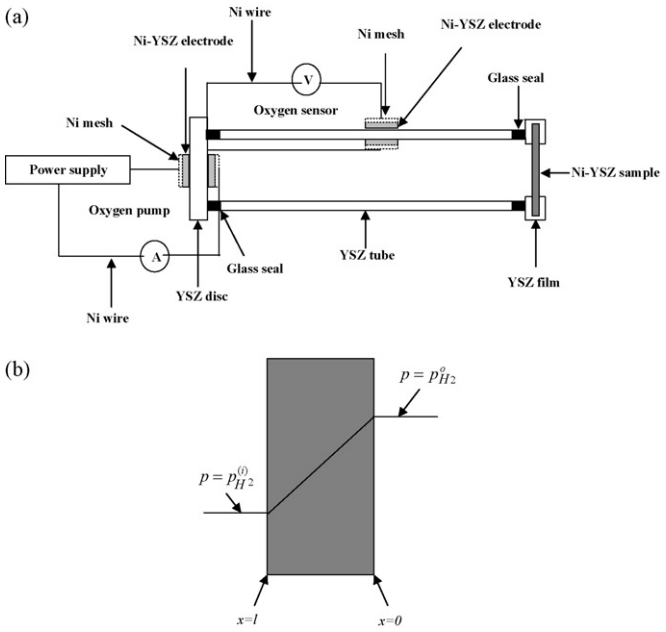

Fig. 1. (a) A schematic of the electrochemical cell to measure the effective binary diffusivity of H_2 and H_2O in porous Ni–YSZ sample. (b) A schematic of Ni–YSZ sample, along with partial pressures of hydrogen.

and 8 mol% YSZ powder [13]. YSZ paste prepared by mixing 8 mol% YSZ powder with a sintering aid, binder, and alpha-terpineol in a desired ratio was painted on the edge of the NiO–YSZ disc to prevent leaks at the edges of the sample and allow gas diffusion through a well-defined area. The open area of the porous sample available for diffusion was 1 cm^2. After drying in an oven, the YSZ disc, YSZ tube and NiO–YSZ disc were sintered at 1300 °C for 2 h in air. Then, Ni meshes connected to Ni wires were attached to the electrodes on the YSZ disc and the YSZ tube using a NiO-based adhesive prepared with NiO powders and Pyro Putty 2400-T (Aremco Products Inc.). The YSZ disc and Ni–YSZ disc were attached to the two ends of the YSZ tube using a glass paste (FuelCellStore). The entire setup was fired at 850 °C under a flow of 300 $cm^3\ min^{-1}$ of humidified forming gas (5% H_2 + 95% Ar) containing 3% H_2O for 4 h to convert NiO to Ni and obtain a leak-tight seal.

The electrochemical cell was place in the furnace, and measurements were performed between 650 and 800 °C with 150 $cm^3\ min^{-1}$ of humidified H_2 containing 3% H_2O using a model 263 A potentiostat from Princeton Applied Research. A constant current in the range 0.01–0.05 A was applied through the YSZ disc to pump the oxygen into the tube, and the Nernst potential of the oxygen sensor was continuously measured until a steady state was established. A steady state is assumed to have been reached when the EMF measured by the oxygen sensor does not change appreciably with time.

After testing, the porous Ni–YSZ sample was sectioned and impregnated with epoxy in vacuum. After the epoxy hardened, it was polished down to a 1 μm finish, and the microstructure and porosity of its cross-section was examined using scanning electron microscopy (SEM).

3. Theoretical analysis

As oxygen is pumped into the YSZ tube, the partial pressure of H_2 inside the tube decreases, and that of H_2O increases. The partial pressure gradients across the porous Ni–YSZ sample generates fluxes of H_2 (J_{H_2}) and H_2O (J_{H_2O}) into and out of the tube, respectively, and in a steady state, the fluxes of H_2 and H_2O across the porous Ni–YSZ sample are related to the flux of O_2 (J_{O_2}) across the YSZ disc by the current density in the oxygen pump (i) as:

$$J_{H_2} = J_{H_2O} = 2J_{O_2} = \frac{i}{2F} \tag{1}$$

where F is the Faraday constant. Since the total pressure is fixed and the fluxes of H_2 and H_2O are in opposite directions ($J_{H_2} + J_{H_2O} = 0$), J_{H_2} and J_{H_2O} can be expressed assuming one-dimensional partial pressure gradients as:

$$J_{H_2} = \frac{i}{2F} = -D^{eff}_{H_2-H_2O}\nabla n_{H_2} = -\frac{D^{eff}_{H_2-H_2O}}{RT}\frac{dp_{H_2}}{dx} \tag{2}$$

$$J_{H_2O} = -\frac{i}{2F} = -D^{eff}_{H_2-H_2O}\nabla n_{H_2O} = -\frac{D^{eff}_{H_2-H_2O}}{RT}\frac{dp_{H_2O}}{dx} \tag{3}$$

where $D^{eff}_{H_2-H_2O}$ is the effective binary diffusivity of H_2 and H_2O in the porous Ni–YSZ sample, n_{H_2} and n_{H_2O} are the concentrations of H_2 and H_2O, respectively, R is the gas constant, T is the temperature, and p_{H_2} and p_{H_2O} are the partial pressures of H_2 and H_2O, respectively. Rearranging and integrating Eqs. (2) and (3) across the porous Ni–YSZ sample:

$$\int_{p^o_{H_2}}^{p^{(i)}_{H_2}} dp_{H_2(a)} = -\int_0^l \frac{RTi}{2FD^{eff}_{H_2-H_2O}}dx \tag{4}$$

$$\int_{p^o_{H_2O}}^{p^{(i)}_{H_2O}} dp_{H_2O(a)} = \int_0^l \frac{RTi}{2FD^{eff}_{H_2-H_2O}}dx \tag{5}$$

where $p^{(i)}_{H_2}$ and $p^o_{H_2}$ are the H_2 partial pressures inside and outside the tube, respectively, $p^{(i)}_{H_2O}$ and $p^o_{H_2O}$ are the H_2O partial pressures inside and outside the tube, respectively, and l is the thickness of the porous Ni–YSZ sample. Fig. 1b shows a schematic of a Ni–YSZ sample, with a thickness and the partial pressures of hydrogen labeled. From Eqs. (4) and (5) and Fig. 1b, the partial pressures of H_2 and H_2O inside the tube at a fixed current density (galvanostatic mode) can be expressed as:

$$p^{(i)}_{H_2} = p^o_{H_2} - \frac{RTl}{2FD^{eff}_{H_2-H_2O}}i \tag{6}$$

$$p^{(i)}_{H_2O} = p^o_{H_2O} + \frac{RTl}{2FD^{eff}_{H_2-H_2O}}i \tag{7}$$

In this experiment, $p^o_{H_2}$ and $p^o_{H_2O}$ are fixed (97% H_2 + 3% H_2O), and $p^{(i)}_{H_2}$ and $p^{(i)}_{H_2O}$ can be determined from the measured Nernst potential using the oxygen sensor on YSZ tube. The Nernst potential, E, is given by

$$E = \frac{RT}{4F}\ln\left(\frac{p^{(i)}_{O_2}}{p^o_{O_2}}\right) \tag{8}$$

where $p^{(i)}_{O_2}$ and $p^o_{O_2}$ are the O_2 partial pressures inside and outside the tube, respectively. Thus, the sensor EMF provides a direct measure of the concentration polarization across the anode at a fixed current density. Once the $p^{(i)}_{O_2}$ is calculated at a fixed current density from the sensor EMF using Eq. (8), $p^{(i)}_{H_2}$ and $p^{(i)}_{H_2O}$ can be obtained using the equilibrium constant (K_{eq}) for the equation $2H_2\ (g) + O_2\ (g) = 2H_2O\ (g)$ (given below in Eq. (9), and the fact that $p_{total} = 1$ atm $\approx p_{H_2} + p_{H_2O}$ everywhere within the anode and inside the YSZ tube; specifically inside the YSZ tube, $p^{(i)}_{H_2O} = 1 - p^{(i)}_{H_2}$.

$$K_{eq} = \frac{p^2_{H_2O}}{p^2_{H_2}p_{O_2}} \tag{9}$$

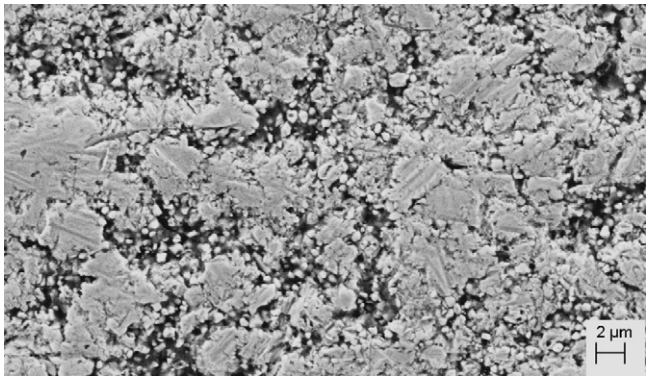

Fig. 2. SEM image of Ni–YSZ anode sample.

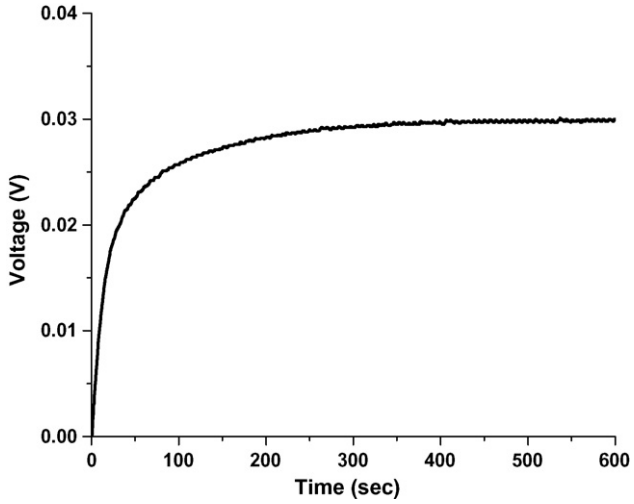

Fig. 3. The Nernst Potential across the oxygen sensor as a function of time at 800 °C with the applied current density of 0.05 A cm^{-2}.

Therefore, $D^{eff}_{H_2-H_2O}$ can be obtained from the slope of either the $p^{(i)}_{H_2}$ vs. i or the $p^{(i)}_{H_2O}$ vs. i plot using either Eq. (6) or (7).

4. Results and discussion

Fig. 2 shows the microstructure of porous Ni–YSZ sample. The thickness was measured to be 750 μm, and the porosity to be 22%. The mean pore size was measured to be 1.3 μm.

Fig. 3 shows typical plot of the measured Nernst potentials as a function of time at 800 °C at a fixed current density of 0.05 A cm^{-2}. Similar measurements were made at 800, 750, 700, and 650 °C between 0.01 and 0.05 A cm^{-2}. The steady state $p^{(i)}_{H_2}$'s were obtained using the measured Nernst potentials and Eqs. (8) and (9) and Fig. 4 shows the $p^{(i)}_{H_2}$ vs. current density plot at 800 °C. The slopes at different temperatures were obtained by fitting into the linear equation, and $D^{eff}_{H_2-H_2O}$'s were calculated using Eq. (6). $D^{eff}_{H_2-H_2O}$ values were 0.070 cm^2 s^{-1} at 800 °C, 0.060 cm^2 s^{-1} at 750 °C, 0.055 cm^2 s^{-1} at 700 °C, and 0.046 cm^2 s^{-1} at 650 °C. In previous studies, $D^{eff}_{H_2-H_2O}$ in the Ni–YSZ anode obtained by fitting i–V curves to the polarization model has been reported to be 0.07–0.82 cm^2 s^{-1} at 800 °C in anodes with volume percent porosity in the range of 23–76% [5,13–16]. In the phenomenological theory of diffusion through porous bodies, the A–B effective binary diffusivity, D^{eff}_{A-B}, is related

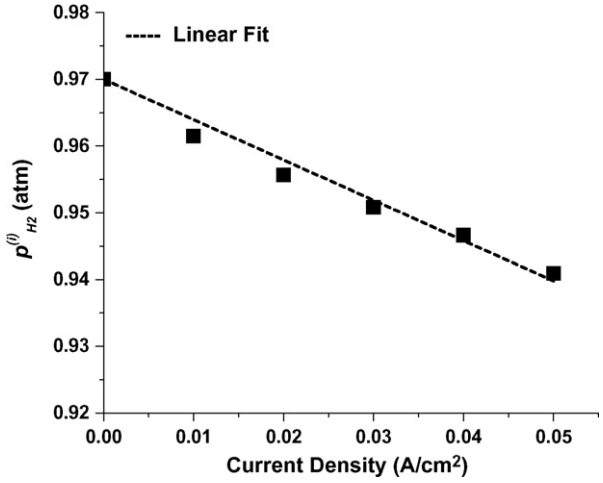

Fig. 4. The H_2 partial pressure inside the tube ($p^{(i)}_{H_2}$) as a function of current density at 800 °C.

to the A–B binary diffusivity, D_{A-B}, by

$$D^{eff}_{A-B} = \frac{V_V}{\tau} D_{A-B} \tag{10}$$

where V_V is the volume percent of porosity, and τ is the tortuosity factor [17]. Eq. (10) shows that the effective binary diffusivity is a function of porosity and tortuosity in the anode, which was systematically studied in our previous study [14]. The diffusivities measured here are smaller than those we have reported previously, presumably because of the lower volume percent porosity in the present anode sample. The Chapman–Enskogg model gives the D_{A-B} as [17]:

$$D_{A-B} = \frac{0.00186\, T^{3/2}((1/M_A)+(1/M_B))^{1/2}}{p\Omega\sigma^2_{A-B}} \tag{11}$$

where M_A and M_B are the molecular weights of the components A and B, respectively, p is the total pressure, Ω is the collision integral, and σ_{A-B} is the collision diameter. Using the Ω and σ_{A-B} data from Cussler [17], $D_{H_2-H_2O}$ is calculated to be 7.6 cm^2 s^{-1} at 800 °C [17], and using the measured volume porosity of the anode and Eq. (10), the tortuosity factor is estimated to be ~22. The tortuosity factor is typically between two and six in porous bodies with a relatively coarse structure, and the value of 21 has been reported on the SOFC anodes with a few microns of pore size and 23% of volume porosity [5,15,17–20]. Although it is difficult to estimate it directly, since the average pore size of the Ni–YSZ sample used in this work was 1.3 μm, the value of ~22 obtained in this work is quite reasonable. Eqs. (10) and (11) show that $D^{eff}_{H_2-H_2O}$ is proportional to $T^{3/2}$, and $D^{eff}_{H_2-H_2O}$ vs. $T^{3/2}$ plot in Fig. 5 shows the linear dependence as expected.

The limiting current density and concentration polarization of the anode can be predicted using the measured $D^{eff}_{H_2-H_2O}$ values to estimate the contribution of the anode concentration polarization to the total performance loss of SOFCs. In operating cells, the anode concentration polarization occurs due to the slow mass transport of gas-phase reactant (H_2) and product (H_2O) species through the porous Ni–YSZ anode, and can be expressed as [5,13–15]:

$$\eta_{a,conc} = -\frac{RT}{2F}\ln\left(1-\frac{i}{i_{as}}\right) + \frac{RT}{2F}\ln\left(1+\frac{p^o_{H_2} i}{p^o_{H_2O} i_{as}}\right) \tag{12}$$

where i_{as} is the anode limiting current density, and $p^o_{H_2}$ and $p^o_{H_2O}$ are the partial pressures of H_2 and H_2O in the anode chamber gas stream, respectively. The anode limiting current density is

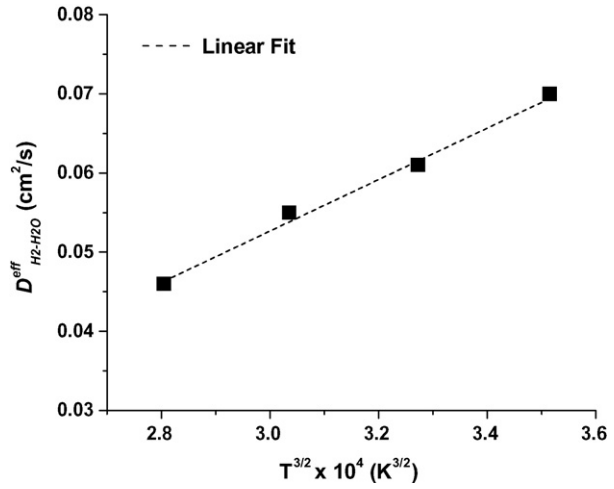

Fig. 5. A plot of $D^{eff}_{H_2-H_2O}$ vs. $T^{3/2}$ between 650 and 800 °C.

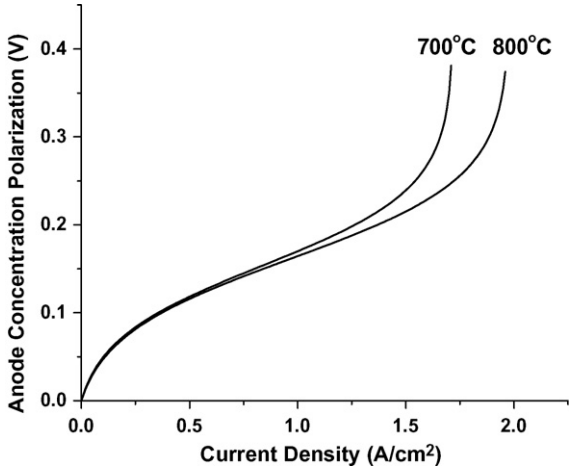

Fig. 6. Anode concentration polarization as a function of current density at 700 and 800 °C calculated using Eq. (12).

the current density at which the hydrogen partial pressure at the anode–electrolyte interface becomes zero, and given by [5,13–15]:

$$i_{as} = \frac{2Fp^o_{H_2} D^{eff}_{H_2-H_2O}}{RTl_a} \quad (13)$$

where l_a is the thickness of the anode. The anode limiting current density can be predicted from experimentally measured $D^{eff}_{H_2-H_2O}$ values using Eq. (13), and they are calculated to be 1.98 A cm^{-2} at 800 °C, 1.78 A cm^{-2} at 750 °C, 1.72 A cm^{-2} at 700 °C, and 1.52 A cm^{-2} at 650 °C. Fig. 6 shows the predicted anode concentration polarization as a function of current density at 700 and 800 °C calculated using the anode limiting current densities and Eq. (12). The anodic concentration overpotentials shown in the figure are a little higher than those we have reported previously, which is due to the fact that the diffusivity measured in the present work is smaller than those of our own estimates from curve fitting voltage–current density curves of single SOFCs made in our lab [14]. The anode concentration polarization can be reduced by increasing the anode porosity and decreasing the thickness. The methodology presented in this paper can be used to characterize the gas transport through the anode and engineer the microstructure. We plan to conduct studies on other SOFC anode materials using this technique and to optimize the anode microstructure and porosity.

5. Conclusion

In this work, the effective binary diffusivity of H_2–H_2O in a porous Ni–YSZ anode was measured using an electrochemical cell under the operating conditions of SOFCs. The effective binary diffusivity of H_2–H_2O was obtained from the relationship between the applied current in the oxygen pump and H_2 partial pressure gradient across the porous Ni–YSZ anode sample measured using the oxygen sensor. The H_2–H_2O effective binary diffusivity values ranged from 0.070 cm^2 s^{-1} at 800 °C 0.060 cm^2 s^{-1} to 0.046 cm^2 s^{-1} at 650 °C. The anode limiting current density and concentration polarization were estimated using the experimental results. Future work will involve improving the anode microstructure to minimize the concentration polarization using the technique presented in this paper.

References

[1] H.P. Buchkremer, U. Diekmann, L.G.J. De Haart, W. Kabs, U. Stimming, D. Stover, Proceedings of the Fifth International Symposium on Solid Oxide Fuel Cells (SOFC-V), Aachen, Germany, 1997.
[2] Y. Patcharavorachot, A. Arpornwichanop, A. Chuachuensuk, Journal of Power Sources 177 (2) (2008) 254.
[3] K. Eguchi, Y. Kunisa, K. Adachi, H. Arai, Journal of the Electrochemical Society 143 (11) (1996) 3699–3703.
[4] H. Yakabe, M. Hishinuma, M. Uratani, Y. Matsuzaki, I. Yasuda, Journal of Power Sources 86 (1–2) (2000) 423–431.
[5] J.-W. Kim, A.V. Virkar, K.-Z. Fung, K. Mehta, S.C. Singhal, Journal of the Electrochemical Society 146 (1) (1999) 69.
[6] E. Ruckenstein, A.S. Vaidyanathan, G.R. Youngquist, Chemical Engineering Science 26 (9) (1971) 1305–1318.
[7] P. Schneider, J.M. Smith, AIChE Journal 14 (5) (1968) 762–771.
[8] P.G. Gray, D.D. Do, AIChE Journal 37 (7) (1991) 1027–1034.
[9] J.R. Hufton, D.M. Ruthven, Industrial & Engineering Chemistry Research 32 (10) (1993) 2379–2386.
[10] F. Zhao, T.J. Armstrong, A.V. Virkar, Journal of the Electrochemical Society 150 (3) (2003) A249–A256.
[11] R.C. Ragan, Process for Producing Low Shrink Ceramic Composition, US Patent, 5,518,969 (1996).
[12] W.C. Belko, R.C. Ragan, Process for Producing Low Shrink Ceramic Bodies, US Patent, 5,769,917 (1998).
[13] K.J. Yoon, S. Gopalan, U.B. Pal, Journal of the Electrochemical Society 156 (3) (2009) B311–B317.
[14] K.J. Yoon, P. Zink, S. Gopalan, U.B. Pal, Journal of Power Sources 172 (1) (2007) 39.
[15] F. Zhao, A.V. Virkar, Journal of Power Sources 141 (1) (2005) 79.
[16] Y. Jiang, A.V. Virkar, Journal of the Electrochemical Society 150 (7) (2003) A942–A951.
[17] E.L. Cussler, Diffusion: Mass Transfer in Fluid System, Cambridge University Press, Cambridge, UK, 1995.
[18] S.H. Chan, K.A. Khor, Z.T. Xia, Journal of Power Sources 93 (1–2) (2001) 130.
[19] H. Zhu, R.J. Kee, Journal of Power Sources 117 (1–2) (2003) 61.
[20] F.P. Reif, Statistical and Thermal Physics, McGraw-Hill, New York, 1975.